GeoInformation in Europe, M.A. Gomarsca (ed.)

The Global Optimal Solution to an inverse model for near-surface velocity from infrared images

Wei Chen, Richard P. Mied & Colin Y. Shen
Naval Research Laboratory, Remote Sensing Division, Washington, D.C. 20375

Keywords: inverse model, surface velocity, infrared images, Global Optimal Solution (GOS)

ABSTRACT: We address the problem of obtaining ocean surface velocities from sequences of thermal (AVHRR) spaceborne images by inverting the heat conservation equation (including sources of surface heat fluxes and vertical entrainment). Instead of AVHRR imagery however, we use the output from a numerical model in this prototype study. Typical formulations of this tracer inversion problem yield too few equations at each pixel, which is often remedied by imposing additional constraints (e.g., horizontal divergence, vorticity, and energy). In contrast, we propose an alternate strategy to convert the under-determined equation set to an over-determined one. We divide the image scene into many sub-arrays, and define velocities and sources within each sub-array using bilinear expressions. A two-dimensional Lagrange spatial interpolation defines the unknowns within each sub-array in terms of the corner points (called knots). In turn, all velocities and sources on the knots can be determined by seeking an optimum solution to these linear equations over the large-scale, which we call the Global Optimal Solution (GOS). We compare the GOS velocity fields with those from the numerical model and from the Maximum Cross Correlation (MCC) technique. The Root Mean Square Error (RMSE) of the two horizontal velocity components between GOS and the numerical model are only the order of one-half ($\Delta t = 1$ hr) and three-quarters ($\Delta t = 4$ hr) those of the MCC-model RMSE. A histogram of the difference between GOS and numerical model velocities is narrower and more peaked than the similar comparison with MCC, irrespective of the time interval between images.

1 INTRODUCTION

Imaging of the world's oceans from space provides large-area synoptic views, and sequential images of the same scene allow us to calculate sea surface velocities. These two-dimensional velocity fields can be very useful in understanding the dynamics of the ocean. Researchers have employed a number of schemes to calculate sea surface velocities from Sea Surface Temperature (SST), but perhaps the two that have received the most widespread use are the Maximum Cross Correlation (MCC) technique of Emery *et al.* (1986) and the heat equation INVerse model (INV) of Kelly (1989). In this work, we are also concerned with inverting the heat equation to obtain the velocity field at the ocean surface.

Since the introduction of the seminal works by Kelly (1989) and Kelly and Strub (1992), the INV technique has been employed and developed in several papers. For example, it has also been employed to infer the properties of the ocean surface mixed layer. Ostrovskii and Piterbarg (1997, 2000) invert an advection-diffusion for the upper ocean mixed layer in different areas of the Pacific Ocean for velocity, as well as vertical mixed layer entrainment velocity and horizontal diffusivity. Using model-generated data, Vigan *et al.* (2000 a, b) demonstrate the utility of the method for the Brazil-Malvinas confluence region, while Zavialov *et al.* (1998) have performed a similar calculation for the same region using SST data mapped from in-situ measurements.

Inversion of the heat equation has proved to be a robust technique that can deliver useful results, but Kelly (1989) points out that the significant science issues must be dealt with first. Specifically, the heat equation is inherently under-determined for the velocity components. Because the velocity field is under-constrained, Kelly adds divergence, vorticity, and energy constraints to obtain a determinate system of equations.

In the present work, we develop the INV technique further by showing that the image scene over which we solve the heat equation may be divided into a number of sub-images. In contrast to previous work, however, we approximate the velocity as a low-order polynomial over each of the subsets. Moreover, we meld the local polynomial fit to each sub-image into a single continuous velocity field for the entire image scene. The velocity is chosen as an optimal fit to the heat equation, and is thus globally valid over the image domain. It is also feasible to group vertical entrainment and diffusive effects into a single function of the horizontal spatial variables, and solve for this field and the velocity simultaneously to yield a Global Optimal Solution (GOS). We evaluate the fidelity of the solutions by comparing them with the output of a three-dimensional, non-hydrostatic numerical ocean model.

2 MODEL AND ALGORITHMS

2.1 *Inverse model equations*

The evolution of the temperature field in a three-dimensional ocean is governed by the heat equation

$$\frac{\partial T}{\partial t} + \mathbf{v}\cdot\nabla T = \kappa\nabla^2 T + S, \tag{1}$$

where $\mathbf{r} = (x, y, z)$ is a position vector, $T = T(\mathbf{r}, t)$ is the temperature field, $\mathbf{v} = \mathbf{v}(\mathbf{r}, t) = (u, v, w)$ is the velocity, and κ is a diffusion coefficient. In the near-surface mixed layer, the variable $S = S(\mathbf{r}, t)$ is a source term containing the effects of air-sea interaction and turbulent processes within the mixed-layer. In this region, the flow is generally modeled as depth independent or locally barotropic, so that an integral over the mixed-layer depth h of Eq. (1) yields

$$T_t + uT_x + vT_y = s, \tag{2}$$

where now, T and (u, v) are functions of only x and y. The term s contains the depth-integrated (and unknown) meteorological forcing and mixed layer entrainment terms (see, e.g., Frankignoul 1985; Ostrovskii and Piterbarg 1995). We have neglected the influence of horizontal diffusion, as it is usually an order of magnitude less than the advective acceleration term (Kelly 1989).

2.2 *Conversion from under-determined to over-determined system*

The temporal and spatial derivatives of the SST fields in equation (2) can be calculated from the mean temperature on the thermal images. The problem is under-determined, however, because three unknowns (u, v, and s) must be derived from a single conservation statement (2) at each of these points.

We show in this section how to use such a representation to obtain an over-determined set of heat equation constraints for the unknown velocity and sources without resorting to additional constraints. To begin, we divide the image scene into a number of $N \times N$ square sub-arrays. Within each of these pixel sub-arrays, such as the one shown in Figure 1, we define the velocities and sources in terms of the corner points (called knots) by

$$(s_{ij}, u_{ij}, v_{ij}) = \sum_{p=0}^{m} \sum_{q=0}^{m} (s_{i_n+np,j_n+nq}, u_{i_n+np,j_n+nq}, v_{i_n+np,j_n+nq}) X_{ijpq}, \tag{4}$$

where X_{ijpq} is a two-dimensional Lagrange polynomial interpolation formula (Press *et al.* 1992) defined by

$$X_{ijpq} = \frac{1}{n^{2m}} \prod_{\substack{k=0 \\ k \neq p}}^{m} (i - i_n - nk) \prod_{\substack{l=0 \\ l \neq q}}^{m} (j - j_n - nl). \tag{5}$$

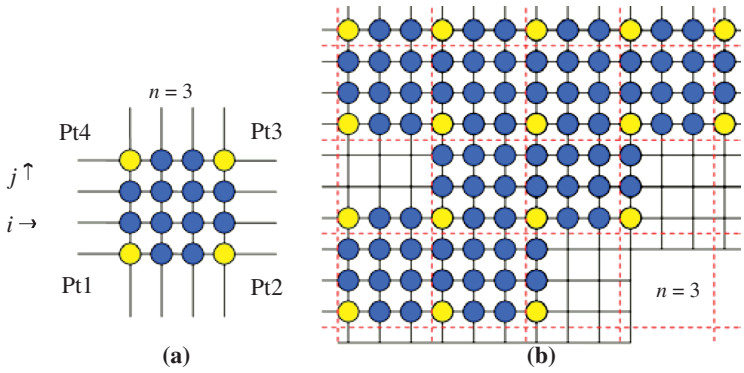

Figure 1. a) A bilinear square grid (m = 1 and n = 3) with four knot points (yellow dots) and twelve interpolation points (blue dots). b) An example of an irregular extended area covered with bilinear square grids.

In (5), i and j are pixel indices over the entire image scene, $i_n = n\,[i/n]$ and $j_n = n\,[j/n]$ are knot indices (where [ ] denotes an integer operator), $n - 1$ is the number of interpolation points between two knots, m is the degree of the polynomials about i and j. The number of knots for a given degree of the interpolation formula is $(m + 1)^2$. An example of bilinear interpolation ($m = 1$) is shown in Figure 1a.

Then, the heat equation (2) in finite difference form for all image pixels $\{i, j\}$ is given by

$$\frac{\partial T_{ij}}{\partial t} = \sum_{p=0}^{m}\sum_{q=0}^{m}\left\{s_{i_n+np,j_n+nq} - u_{i_n+np,j_n+nq}\left(\frac{\partial T_{ij}}{\partial x}\right) - v_{i_n+np,j_n+nq}\left(\frac{\partial T_{ij}}{\partial y}\right)\right\}X_{ijpq} \tag{6}$$

The over-determined system (6) can be solved by a least-squares method on a square grid if the number of unknown parameters, $3 \times (m + 1)^2$, is less than the number of equations, or $(n + 1)^2$.

2.3 *Global Optimal Solution*

By imposing these square grids over the entire image area and adapting the indexing scheme appropriately, we can extend the optimal problem from the local to global, as shown in the bilinear example in Figure 1b. The grids can assembled to form an arbitrary shape, in which a linear equation system with variables at knot points can be solved uniquely if total number of pixels in selected area is greater than three times the total number of knots. An inversion of the heat equation thus becomes a global linear optimization problem, and a velocity field and pseudo-sources on knots can be obtained over the whole image by solving a linear equation system.

3 MODEL AND MCC COMPARISON

To assess the ability of the present method to obtain surface velocities, we use the solution of a numerical model as a benchmark, and also use this solution to compare the accuracy of our result to that of MCC.

3.1 *The numerical model*

A simulated flow field and its advection of sea surface temperature are obtained by solving the following three-dimensional nonlinear fluid dynamical equations and the equation for temperature. For the purposes here, the temperature T is treated simply as a passive tracer with a weak diffusivity added for numerical stability. The solution procedure is the same as that given in Shen and Evans (2002), and is based on a pseudo-spectral calculation. The three-dimensional (3D) domain of this model has a rigid flat surface at the top and bottom and open periodic boundary conditions on the four sides. The horizontal dimension of the model domain is L = 50 km. The depth of the domain is at 30 m, and the horizontal resolution (0.521 km) results from an evenly spaced grid with 96 points on each side.

3.2 *The GOS result and comparison to MCC*

In the calculations reported here, only the bilinear interpolation polynomial ($m = 1$) is used in each array to connect the four corner-points or knots to the other points (see Figure 1a). An example of the velocity vectors obtained from GOS is shown in Figure 3b; and for comparison, the benchmark velocity vectors given by the numerical model are shown in Figure 2a. The sub-arrays used to obtain this GOS result are $n = 10$ grid points wide on each side. The two velocity vector fields in Figure 2 exhibit strong similarities.

In Figure 3c, d, the root-mean-square magnitude difference between the model and GOS velocities is shown as a function of n for $\Delta t = 1$ hr (Figure 3c) and $\Delta t = 4$ hr (Figure 3d). We denote the difference in magnitude between the model and MCC by the horizontal line in each panel.

To further examine the accuracy of GOS and MCC results, histograms of the errors in speed and direction are shown in Figure 4a, b. Compared with the MCC vectors, the GOS histograms are generally narrower, have higher amplitude, and are more closely centered on zero. The only exception to this is the velocity magnitude histogram for the $\Delta t = 4$ hr result (Figure 4c). There, it is evident that the MCC and GOS histograms have comparable height and width, but with peaks displaced from $\Delta V = 0$ by approximately the same amount.

For velocity vectors generated with $\Delta t = 1$ hr, the GOS method is substantially more accurate than the MCC (Figure 4a, b). However, this disparity decreases when $\Delta t = 4$ hr, and these similarities and differences can again be explained by considering the time interval Δt and pixel size. As discussed for Figure 4a, b, representative particle

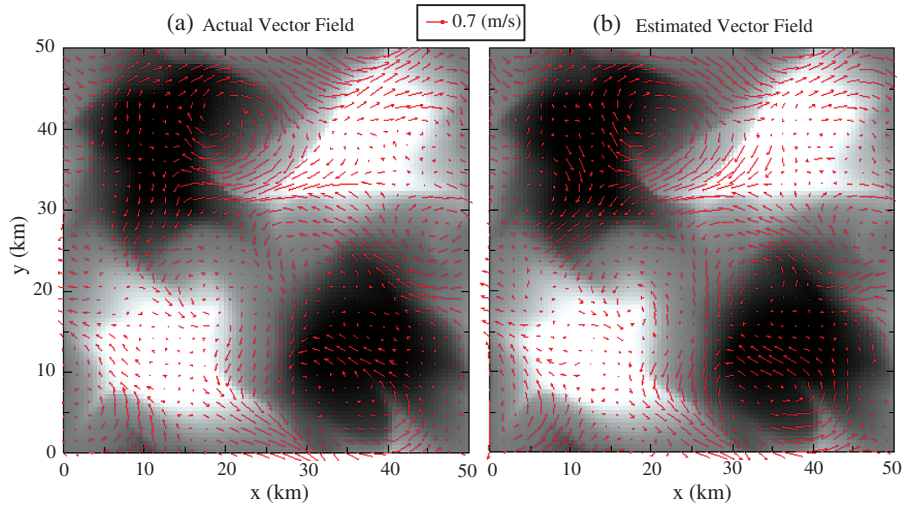

Figure 2. Velocity fields. a) Average of the actual vector fields generated by the model at times $t_1 = 3$ hr and $t_2 = 4$ hr. b) Estimated vector field obtained from the GOS between times t_1 and t_2. Vectors are plotted every three pixels.

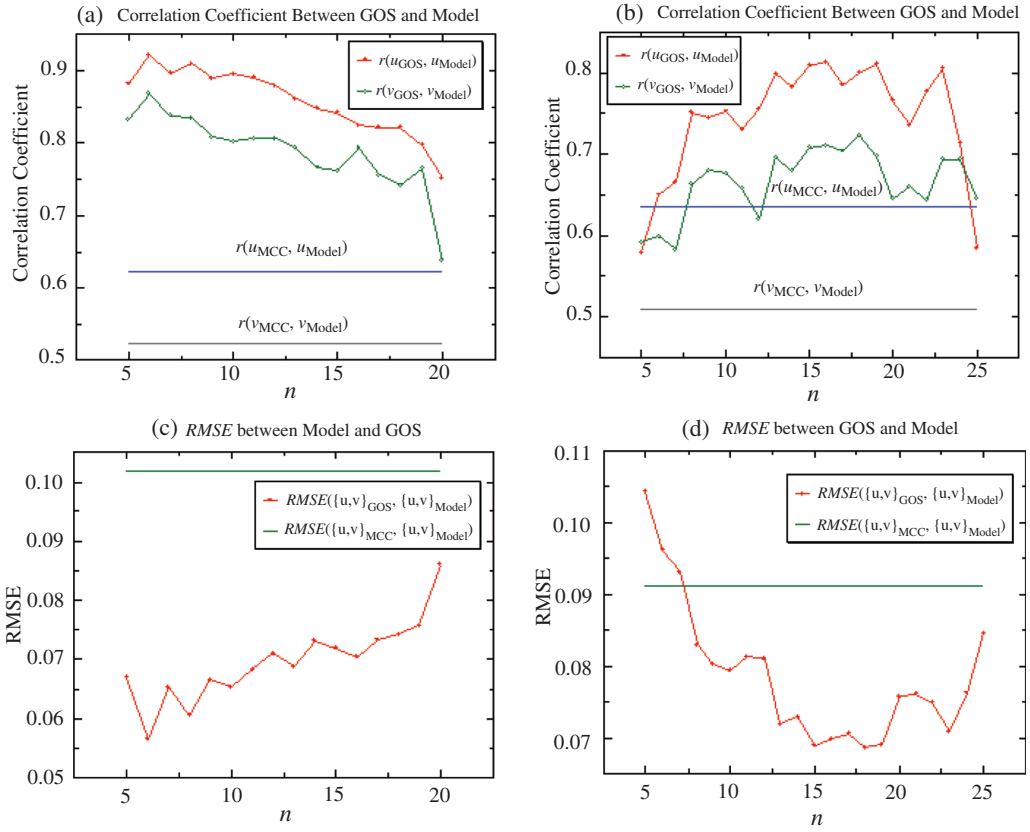

Figure 3. (a) and (b) Correlation coefficients of velocity components u and v vs. the number of interpolation points by GOS with $\Delta t = 1$ hr. (c) and (d) Root Mean Squares Error (RMSE) of velocity components u and v and vs. the number of interpolation points by GOS with $\Delta t = 4$ hr.

displacements in the case $\Delta t = 1$ hr are the order of only 4 pixels. Because the MCC calculation can discern position only in increments of integral pixels, this number can easily be in the 3–5 pixel range, for an error of 20–25%. In contrast, the GOS technique calculates a displacement in terms of actual distance (km), and is not subject to this error. For larger times (e.g., $\Delta t = 1$ hr) the displacements are commensurately larger, and the disparity between the two techniques is not as pronounced. Nevertheless, the GOS has an advantage for this larger time increment as well. While the GOS and MCC yield comparably accurate velocity magnitudes (Figure 4c), the angles of the GOS velocity vectors are more accurate than those from MCC. Figure 4d shows that the GOS histogram is narrower and more sharply peaked than the GOS one, indicating the greater accuracy of the GOS velocity directions.

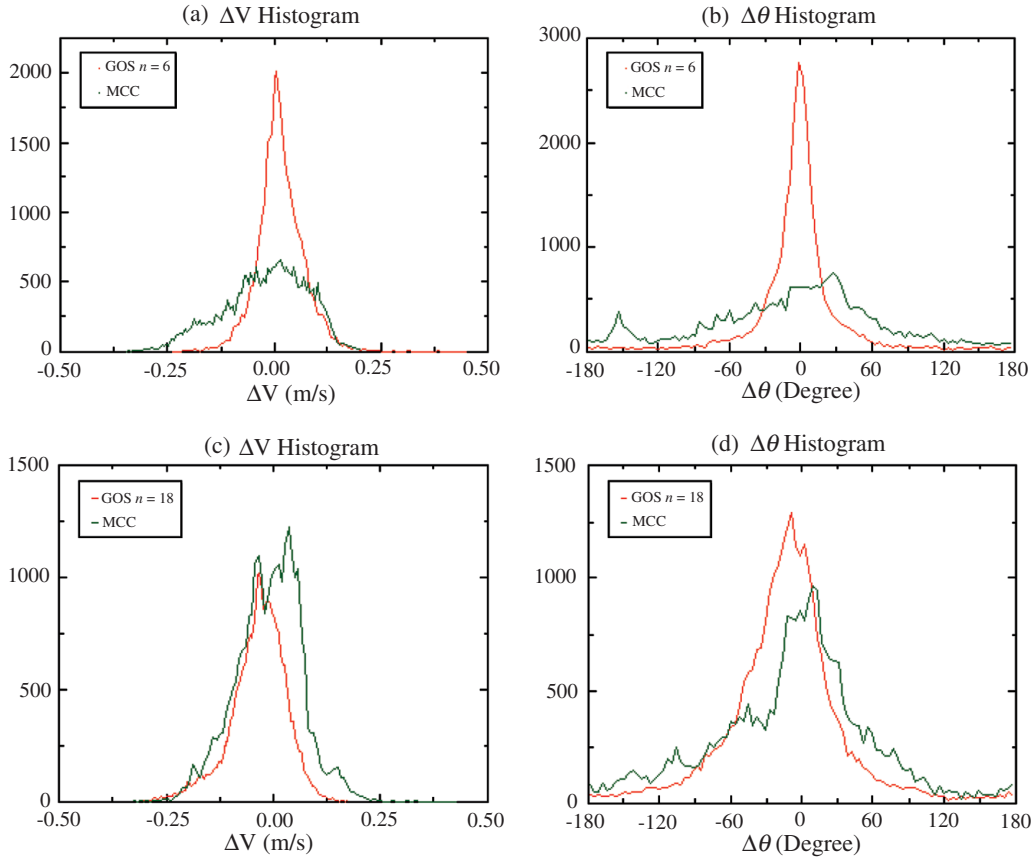

Figure 4. Histograms of magnitude and angle differences between the Ocean Model velocities and those from both GOS and MCC. Image sequence times are (a) and (b) with $\Delta t = 1$ hr, and (c) and (d) with $\Delta t = 4$ hr. For comparison, the total number of vectors estimated by GOS and MCC in these figures are equal.

4 CONCLUSIONS

We have presented a new Global Optimal Solution (GOS) to an inverse model to obtain near-surface velocity from sequential infrared images. The surface velocities on the corner points (knots-see Figure 1) of each tile can be solved for simultaneously by an over-determined linear equation system derived from a global optimization requirement. We compare the GOS velocity fields with those from the numerical model and the MCC technique. Root Mean Square Error (RMSE) of two velocity components between GOS and the numerical model are only the order of one-half ($\Delta t = 1$ hr) to three-quarters ($\Delta t = 4$ hr) those of MCC (Figure 3c, d). A histogram of the difference between GOS and numerical model velocities is narrower and more peaked than that with the MCC-model comparison (Figure 4).

ACKNOWLEDGEMENT

This research work was supported by the Office of Naval Research through the project WU-8743-07 at the Naval Research Laboratory.

REFERENCES

Emery, W.J., Thomas, A.C., Collins, M.J., Crawford, W.R. & Mackas, D.L. 1986. An Objective Method for Computing Advective Surface Velocities from Sequential Infrared Satellite Images, *Journal of Geophysical Research* 91, 12865–12878.

Frankignoul, C. 1985. Sea surface temperature anomalies, planetary waves, and air-sea feedback in the middle latitudes, *Journal of Geophysical Research* 23, 357–390.

Kelly, K.A. 1989. An Inverse Model for Near-Surface Velocity from Infrared Images, *Journal of Physical Oceanal Graphy* 19, 1845–1864.

Kelly, K.A., Strub, P.T. 1992. Comparison of Velocity Estimates from Advanced Very High-Resolution Radiometer in the Coastal Transition Zone, *Journal of Geophysical Research* 97, 9653–9668.

Ostrovskii, A., Piterbarg, L. 1995. Inversion for Heat Anomaly Transport from Sea-Surface Temperature Time-Series in the Northwest Pacific, *Journal of Geophysical Research* 100, 4845–4865.

Ostrovskii, A.G., Piterbarg, L.I. 2000. Inversion of Upper Ocean Time Series for Entrainment, Advection, and Diffusivity, *Journal of Physical Oceanal Graphy* 30, 201–204.

Press, W.H., Teukolsky, S.A., Vetterling, W.T. & Flannery, B.P. 1992. Numerical Recipes in C, Cambridge University Press, 2nd Edition, 108–123.

Shen, C.Y., Evans, T.E. 2002. Inertial instability and sea spirals, *Geophysical Research Letters,* 29 (23), 2124, doi: 10.1029/2002GL015701.

Vigan, X., Provost, C., Bleck, R.R. & Courtier, P. 2000. Sea Surface Velocities from Sea Surface Temperature Image Sequences. 1. Method and validation using primitive equation model output, *Journal of Geophysical Research* 105, 19499–19514.

Vigan, X., Provost, C., Bleck, R.R. & Courtier, P. 2000. Sea Surface Velocities from Sea Surface Temperature Image Sequences. 2.Application to the Brazil-Malvinas Confluence Area, *Journal of Geophysical Research* 105, 19515–19534.

Zavialov, P.O., Ghisolfi, R.D. & Garcia, C.A.E. 1998. "An Inverse Model for Seasonal Circulation over the Southern Brazilian Shelf: Near-Surface Velocity from the Heat Budget", *Journal of Physical Oceanal Graphy* 28, 545–562.